NANO LETTERS

pubs.acs.org/NanoLett Letter

Tailored Fabrication of 3D Nanopores Made of Dielectric Oxides for Multiple Nanoscale Applications

German Lanzavecchia, Anastasiia Sapunova, Ali Douaki, Shukun Weng, Dmitry Momotenko, Gonçalo Paulo, Alberto Giacomello, Roman Krahne,* and Denis Garoli*

Cite This: https://doi.org/10.1021/acs.nanolett.4c02117 Read Online

ACCESS | Metrics & More | Article Recommendations | Supporting Information

ABSTRACT: Solid-state nanopores are a key platform for single-molecule detection and analysis that allow engineering of their properties by controlling size, shape, and chemical functionalization. However, approaches relying on polymers have limits for what concerns hardness, robustness, durability, and refractive index. Nanopores made of oxides with high dielectric constant would overcome such limits and have the potential to extend the suitability of solid-state nanopores toward optoelectronic technologies. Here, we present a versatile method to fabricate three-dimensional nanopores made of different dielectric oxides with convex, straight, and concave shapes and demonstrate their functionality in a series of technologies and applications such as ionic nanochannels, ionic current rectification, memristors, and DNA sensing. Our experimental data are supported by numerical simulations that showcase the effect of different shapes and oxide materials. This approach toward robust and tunable solid-state nanopores can be extended to other 3D shapes and a variety of dielectrics.

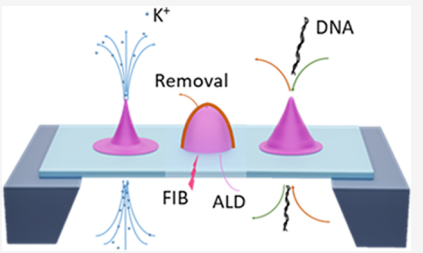

KEYWORDS: *solid-state nanopores, 3D fabrication, single-molecule sensing, memristors, ICR*

Over recent decades, key advancements in nanopore technology have paved the way for improved applications in various fields, including sequencing,[1] biosensing,[2,3] nanofluidics,[4] ion transport[5] and selectivity,[6] electro-osmosis,[7] energy harvesting,[8−10] and electronic devices.[11,12] Notably, nanopores offer direct physical access to biomolecule analysis[13,14] and play a pivotal role in third-generation sequencing[15] and DNA data storage.[16] However, challenges persist in nanopore technology, including limited pore lifetime and stability,[17] difficulties in tuning pore size,[18] limited selectivity, and scalability from single pores to pore array configurations. Solid-state nanopores,[19,20] in particular, have become the focus in single-molecule sensing due to their high robustness and durability,[21] even under harsh conditions in terms of temperature, pressure, and pH. Various fabrication approaches have been developed,[22] utilizing a wide range of materials, wherein the shape and size of the nanopores are defined by the fabrication method.[8]

The geometric distribution of charges inside the nanopore, determined by the surface charge of the material and by the 3D shape of the nanochannel,[23,24] can have important effects on the nanopore's functionality. Depending on the shape and material of the nanopore, the inner surface charges influence the ion concentration and electrostatic potential inside the nanopore.[25] This leads to ionic current rectification (ICR),[26,27] with highly asymmetric nanopores producing high ICR ratios.[28] Moreover, the nanopore conductance can depend on the behavior of the surface charges that redistribute within the nanopore channel due to the finite mobility of ions under applied potentials,[29,30] which leads to memristive behavior, as discussed in some recent works.[31,32]

The choice of material and geometry can also influence the noise in nanopore ionic current measurements.[19,33,34] For example, quartz nanopipettes have been employed to measure the current blockade of geometrical features separated only by 6 nm along a DNA strand,[35] attributing this super-resolution to the enhancement of the electric field at the tip of the nanopore. However, a quartz nanopipette limits the application to a single nanopore. On the contrary, nanopores on a silicon chip[36] can be fabricated as nanopore arrays[37] for parallel and high-throughput applications. In this view, HfO_2 (hafnium dioxide) step-like conical nanopore arrays on Si_3N_4 membranes have been recently fabricated for biosensing and energy harvesting, using a modified atomic layer deposition (ALD) configuration.[8] Taking inspiration from this work, we present a robust method to fabricate three-dimensional on-chip nanopores with arbitrary geometries made of different dielectric oxides. These structures can be readily realized on solid-state substrates (on-chip) and fabricated as single pores, as pore arrays, or in arbitrary arrangements. The fabrication is based on focused ion beam (FIB) lithography that produces a hollow

Received: May 7, 2024
Revised: June 18, 2024
Accepted: June 21, 2024

conical structure of a photoresist mold onto a silicon/silicon nitride chip.[38] Then the metal oxide is deposited from the back side of the membrane by ALD or physical vapor deposition (PVD).[39] The crucial step is the full removal of the hardened photoresist that we achieved by UV light exposure (to break the cross-linking of the polymer chain in the resist) followed by low-power oxygen plasma in our reactive ion etching with inductively coupled plasma (ICP-RIE) setup or by heating the samples to 600 °C under an O_2 atmosphere. With this process, we obtain nanopores with few nanometer apertures consisting only of the metal oxide, while their shape can be controlled in 3D by FIB lithography.[40] We demonstrate the fabrication of nanopores from four different oxides (SiO_2, Al_2O_3, TiO_2, and HfO_2) and three different shapes (with concave, convex, or straight edge profiles) and investigate their performance in ICR and single-molecule detection and as ionic memristors.[39,27]

Figure 1 depicts the three different conical nanopore shapes fabricated on a silicon nitride membrane that we discuss in this

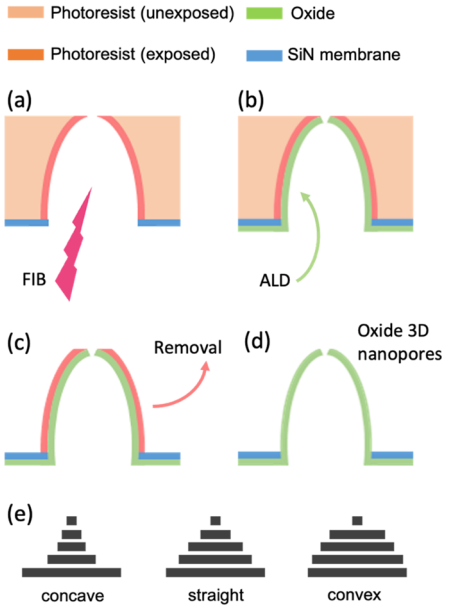

Figure 1. 3D oxide nanopore fabrication illustrated in cross-sectional schemes. (a) A photoresist layer on a SiN membrane is milled by FIB lithography from the backside, resulting in a thin layer of hardened resist. The oxide material is deposited by ALD as a thin layer (b), and then the photoresist is removed using standard solvents (c) leaving the hardened layer behind, which is removed by UV exposure and oxygen plasma or thermal annealing at high temperature (d). (e) Different nanopore shapes are obtained by concentric disk exposure in the FIB lithography.

work. The fabrication process is described in Figures S1 and S2, and scanning electron microscope (SEM) images of the differently shaped 3D nanopores are shown in Figure 2. We report several additional examples of single nanopores and nanopore arrays in the Supporting Information in Figures S3 and S7 to demonstrate the versatility of the method. The key features are the deposition of the photoresist from the top side, with the successive FIB lithography and metal oxide deposition from the backside of the membrane. This combination retains the freedom in the design of the nanopore of the FIB lithography and enables the full removal of the photoresist mold after metal oxide deposition. An additional advantage of the approach is that the nanopore aperture can be defined with nanometer resolution by the fine thickness control of the ALD of the dielectric metal oxide. To fabricate 3D hollow conical structures with different edge profiles in the photoresist, we adapted a technique based on FIB milling of concentric disks with different diameters; see Figure S2 for details.[38,41,42] Here the secondary radiation and electron scattering related to the ion-beam exposure results in cross-linking of the photoresist in the vicinity of the removed disk volume, which leads to a layer of hardened photoresist with ca. 50 nm thickness that wraps the external shape of the disk stacks. This photoresist mold is then used as a template for the dielectric oxide nanopores.

We note that we distinguish here two different photoresist thicknesses: one is the overall layer thickness after spin coating in the micrometer range, defining the height of the 3D-nanopore; the other is the thickness of the cross-linked photoresist layer. The metal oxide can be deposited by PVD or ALD. PVD can be directly applied to the samples since the process is directional and therefore covers only the backside of the membrane and the photoresist cones. However, PVD films are slightly grainy, and therefore, this approach provides only limited control on the nanopore diameter, with the risk of blocking the opening. With ALD, very homogeneous layers with high control on thickness can be obtained,[40] but it is important to ensure one-sided deposition to be able to remove the photoresist mold. To achieve this, we place the sample top side down on a polydimethylsiloxane (PDMS) substrate that adheres to the photoresist and protects the top side from the ALD, while leaving the backside accessible for metal oxide deposition. Thermal ALD is preferred over plasma ALD, as it produces higher quality oxide layers[43,44] and does not contribute to further hardening of the photoresist that would make the resist removal more difficult.

The removal of the hardened photoresist mold is challenging.[45,46] Standard oxygen plasma processes do not work, as they only reduce the thickness[45] to a persistent layer of around 30 nm.[47] Solvents such as *N*-methyl-2-pyrrolidone (NMP), designed to remove hardened photoresist, prove ineffective in the complete elimination of this layer. We tested piranha solution as an additional etchant, but this resulted in membrane damage, and aggressive oxygen plasma treatments performed in an RIE-ICP configuration led to damage of the thin dielectric layers. We found that resist removal using UV light to break the cross-linking in the photoresist[45,47] followed by low-power oxygen plasma in an ICP-RIE leads to fast and effective removal of the photoresist. Another successful strategy that we applied for resist removal is thermal annealing at 650 °C in the presence of oxygen, which facilitates the decomposition and degassing of organic materials[48] and concurrently improves the mechanical and optical properties of the oxide layer.[49,50] Both methods proved to be effective in fully removing the hardened photoresist layer, as confirmed by the EDS mapping shown in Figure 2e–g.

The metal deposition by ALD on a mold gives access to a wide variety of dielectric oxides as materials for 3D nanopores. We tested all materials available in our ALD system, which are SiO_2, Al_2O_3, TiO_2 (titanium dioxide), and HfO_2 ; see Figure 2 and Figures S6 and S7 in the SI. This set of dielectric oxides outlines the flexibility of our fabrication that allows selecting the nanopore material to meet specific application requirements, in particular toward high dielectric constant materials that can open up possibilities to integrate nanophotonic resonators and Mie-tronics in the nanopore platform.[51,52]

https://doi.org/10.1021/acs.nanolett.4c02117
Nano Lett. XXXX, XXX, XXX−XXX

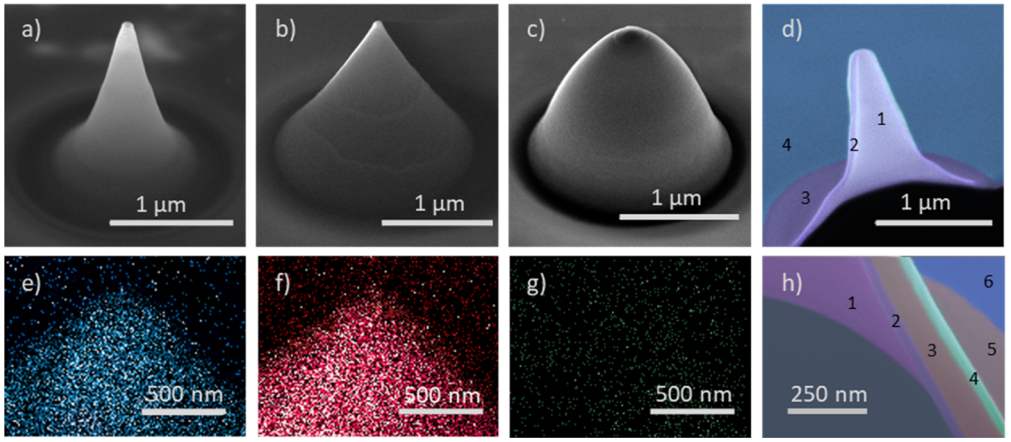

Figure 2. Electron microscopy analysis of metal oxide nanopores with different shapes. SEM micrographs of Al_2O_3 nanopores with concave (a), straight (b), and convex (c) edge profiles. The aperture of the nanopores is around 30 nm in all cases. (d) Cross section of a concave Al_2O_3 nanopore (marked 1, interior wall of the nanopore in SiO_2; 2, cross section of the dielectric wall; 3, outer SiO_2 wall; 4, Si_3N_4 membrane). (e–g) Compositional analysis of an Al_2O_3 nanopore by electron dispersive spectroscopy (EDS) mapping, showing the signals for Al (e), O (f), and C (g). (h) Cross section of a convex SiO_2 nanopore before photoresist removal; the SiO_2 and photoresists section are highlighted by false colors (marked 1, interior wall of the nanopore in SiO_2; 2, cross section of the dielectric wall; 3, cross section of the photoresist wall; 4, Pt layer; 5, outer photoresist wall; 6, Si_3N_4 membrane).

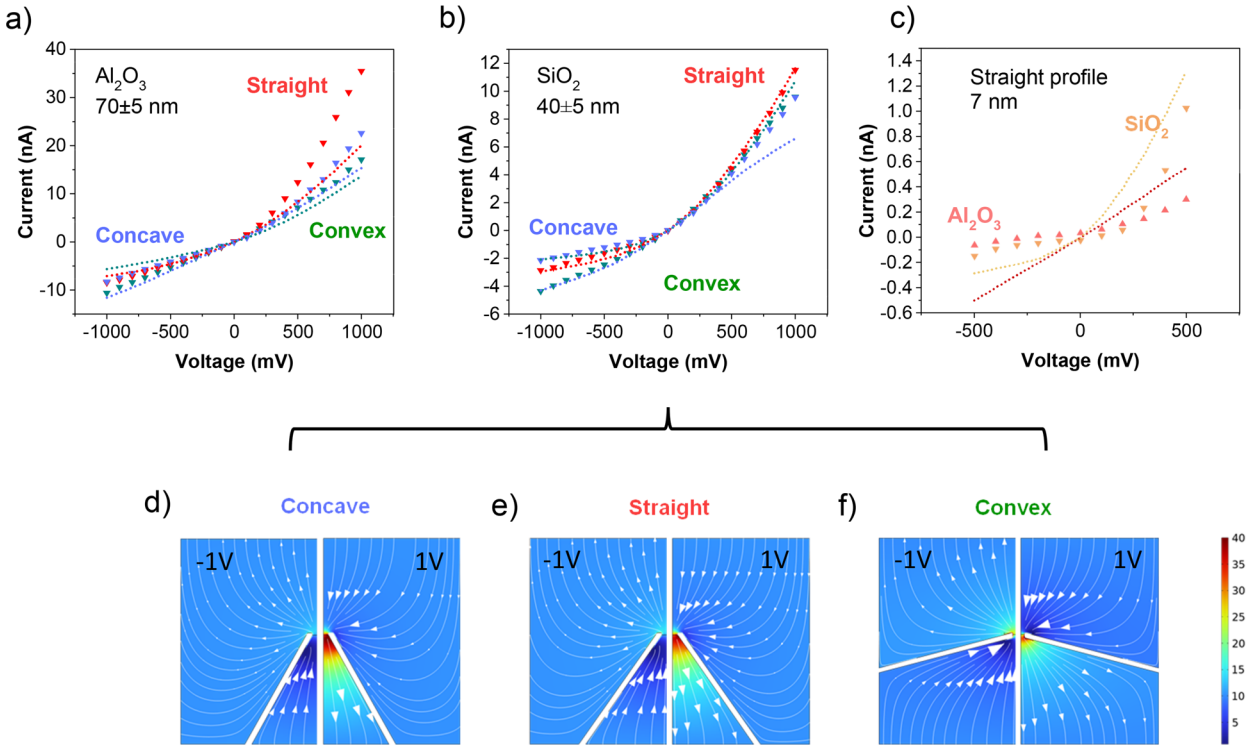

Figure 3. Ionic current rectification: measured (triangles) and simulated (dotted lines) $I-V$ characteristics of the three nanopore geometries in a 10 mM KCl electrolyte. (a–c) Current voltage curves for nanopores with different shapes and materials as described in the legends. (d–f) Simulated concentration profiles of K^+ [mol/m^3] and total flux (streamlines) for a SiO_2 nanopore with 40 nm diameter with (d) concave, (e) straight, and (f) convex profile.

Now we turn to explore the properties and functionality of the all-dielectric oxide nanopores in a range of applications, which are ICR, single-molecule detection, and as memristors. In this respect, we take advantage of the design freedom that our fabrication provides and investigate the impact of the different oxide materials (SiO_2, Al_2O_3), different nanopore shapes (with concave, convex, and straight profiles), and pore diameters (ranging from 7 to 70 nm).

ICR depends on the nanopore shape, size, and surface properties.[53] Figure 3a shows the conductance (in 10 mM KCl electrolyte) of Al_2O_3 nanopores that have different shape, but a similar channel length of 1.4 μm and pore diameter of around 70 nm. ICR is observed for all three shapes with a higher current at positive bias with respect to negative bias, and this effect is strongest for the pores with straight profiles. We observe a similar behavior for SiO_2 nanopores with about 40 nm pore diameter, as depicted in Figure 3b. As could be

https://doi.org/10.1021/acs.nanolett.4c02117
Nano Lett. XXXX, XXX, XXX−XXX

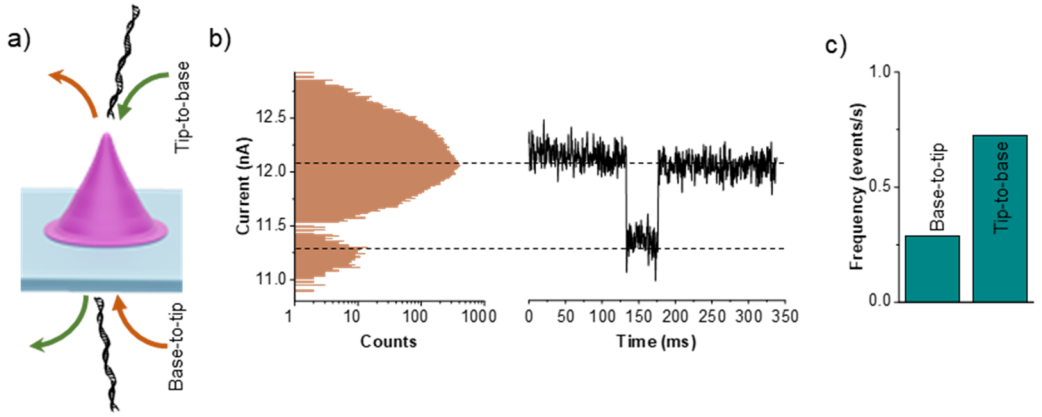

Figure 4. (a) Schematic layout of the DNA translocation experiments. (b) Current blockade histogram of λ-DNA translocations through a straight profile nanopore in 1 M KCl at V = 500 mV, measured at 20 kHz, with a characteristic translocation event on the right. (c) Relative frequencies of DNA translocation events in tip-to-base and base-to-tip directions.

expected, the 3D nanopores exhibit strong rectification with typical ICR ratios in the range between 4.6 and 1.6, which is significantly higher than ICR in planar pores that typically have ICR ratios around 1.

Our smallest nanopores with opening diameters of around 7 nm exhibit even stronger ICR. Figure 3c exemplifies the $I-V$ curves for straight pore shapes fabricated with SiO_2 and Al_2O_3. In such narrow nanopores, the movement of the ions is dominated by the surface charge; thus the rectification effects are enhanced, and we obtain ICR (at 500 mV) ratios of 7.0 for SiO_2 and 4.9 for Al_2O_3, whereas values reported for conical nanopores in a SiO_2 membrane are in the range of 1−2.[54]

To elucidate the fact that pores with straight profiles feature stronger ICR than concave or convex shapes, we performed finite element method modeling (COMSOL Multiphysics version 5.3). The Poisson−Nernst−Planck (PNP) equations[55,56] were employed to describe distributions of electric potential and ionic species concentrations across the entire domain, as well as to simulate respective ionic fluxes. Further details can be found in Section 3 in SI. As shown in Figure 3d−f, which depicts the magnified view on the pore tip region for concave, straight, and convex geometries, the major difference between the shapes is the value of the half-cone angle in the vicinity of the opening. This angle typically reaches 15−30° for concave, 30−45° for straight, and 70−80° for convex nanopores and has a pronounced effect on local ionic distributions and ionic conductivity. As the angle of the nanopore increases from concave to straight and then to convex shapes, a corresponding reduction in the conductivity asymmetry at opposite bias polarities can be observed. This consequence of a smaller accumulation and depletion of ionic species at the tip of the nanopore at higher cone angles is related to a reduced asymmetry of the mass transport between the inner and outer parts of the nanopore. Inside the pore, the mass transport is rather restricted and allows for stronger ion accumulation or depletion (depending on bias polarity), which also strongly depends on the cone semiangle, whereas the mass transport outside the pore remains mainly unchanged. These variations in the geometry cause a major effect on ICR,[24,57,58] with stronger mass-transport asymmetry (inside vs outside of the pore) that causes more intense high and low conductance states at opposite biases for concave, rather than straight, or even convex pore shapes.

Further differences between the fabricated nanopores are related to the magnitude of the surface charges, which are directly related to the choice of the pore material. We note that we needed to assign negative surface charges to accurately reproduce our experimental results, in contrast to other reports.[59] This difference most likely originates from impurities or structural differences induced by the deposition process that favors deprotonation of hydroxyl groups on the aluminum surface, rendering the surface negative. The surface charge can dependon the fabrication methods, chemical functionalization of the pore walls, and interactions between surface groups and ions in the electrolyte solution due to acid−base (pH) or other equilibria.[54,60] In this regard, the main difference between Al_2O_3 and SiO_2 nanopores is in their surface charge. In our ICR simulations, we assigned surface charges from −0.02 to −0.04 C/m^2 and from −0.06 to −0.1 C/m^2 for SiO_2 and Al_2O_3 nanopores, respectively, thus resulting in a different degree of ICR. Therefore, the nanopore fabrication concept developed in this work offers a versatile platform to manipulate ICR in a wide range of conditions, from geometry to nanopore materials.

Figure 4 reports the properties of the nanopore in single-molecule sensing, implemented by electrical detection of the translocation of single λ-DNA molecules in 1 M KCl solution through the nanopore in a nanopore reader.[61] The conical shape improved the overall signal-to-noise ratio compared to our previous work[62] with cylindrical nanopore geometry. The conical shape resulted also in an asymmetry as compared to to the direction of translocation in terms of both frequency of events and signal-to-noise; that is, the relative signal was $\Delta I/I_0$ = 8% for base-to-tip and $\Delta I/I_0$ = 11% for tip to base translocations (Figure 4a), and we observed approximately twice the amount of translocation events in the tip-to-base direction with respect to the base-to-tip direction (Figure 4c). This is in agreement with recent results reported in glass nanopipets[35] and HfO_2 step-like conical nanopores and most likely originates from the nonuniform electric field distribution and the electroosmotic flow that the DNA molecule must overcome in the translocation process.[8]

Ionic memory resistors (memristors) promise groundbreaking advancements in neuromorphic technologies[63−65] by exploiting their capability to unite computing and memory in the same element. The conductance of ionic memristors at a given bias voltage depends on the preceding voltage bias

https://doi.org/10.1021/acs.nanolett.4c02117
Nano Lett. XXXX, XXX, XXX−XXX

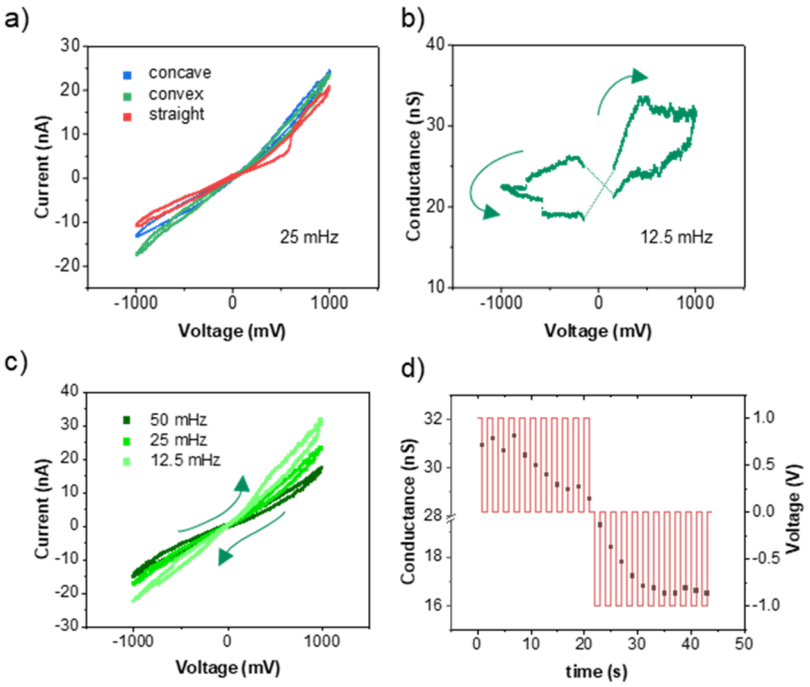

Figure 5. (a) Memristive behavior of the SiO_2 3D nanopores during cyclic ramp voltammetry in a 200/20 mM (tip side/base side) KCl gradient. (b) Conductance of a conical pore of convex profile, showing the typical crossing of unipolar pores. The conductance curve is such that it decreases when the applied voltage increases; switching behavior occurs when the sign of the voltage is changed. (c) Memristive response depending on the cycling frequency. Here we show that the area of the hysteresis loop of a conical pore of the convex profile increases with lower cycling frequencies. (d) Change in the conductivity (black) of the 50 nm concave pore as a series of 1 s voltage pulses (red) is applied. These pores show a "learning" behavior, where the conductivity decreases as more pulses are applied.

events; that is, the conductance bears memory of the recent history of bias voltages across the ionic memristor. This memory effect observed in memristors is reminiscent of short-term synaptic plasticity in neurons, where the response of a neuron after a synapse depends on the history of the activations before the synapse.[66,67]

Figure 5 reports the $I-V$ curves of cyclic voltammetry in conical 3D nanopores. These plots show the pinched hysteretic behavior that is the fingerprint of memristors.[68] Figure 5a shows the hysteretic behavior of the three types of conical pores. Although there are significant differences between shapes, we observe qualitatively the same behavior with an open hysteresis loop in the $I-V$ (Figure 5a) that leads to a crossing at around zero bias voltage in the conductance–voltage curve (Figure 5b). This memristive behavior is similar to that reported in the literature for larger, concave pores,[12,69] and its origin stems from the transient concentration polarization that is due to the asymmetry of the pores, their conical shapes, and their charged surfaces. Significant theoretical work has been done to estimate the diffusion limited memory time scale of the hysteretic loop, which should scale as $\frac{L^2}{D}$, where L is the channel length of the pore and D the ionic diffusivity coefficient.[70,71] Using L = 1.4 μm and $D = 1.4\frac{\mu m^2}{ms}$ yields time scales on the order of milliseconds, thus orders of magnitude faster than the behavior that we observe in Figure 5c,d that is in the range of several tens of seconds. We therefore think that the trapping and detrapping of surface charges in the channel are at the origin of the memristive behavior that we observe.

As an additional characterization of the memristor behavior, we show, in Figure 5d, an experiment in which the nanopores are subjected to a series of positive voltage pulses followed by negative ones. The pulses produce a synaptic-like decrease of the conductance for both positive and negative pulses, consistent with a unipolar memristor. This means that the nanopore effectively "remembers" the previous pulses and that its downstream conductance can be "programmed" by providing an appropriate train of pulses. This behavior suggests that nanopores of this kind could be employed as elements of nanofluidic neuromorphic circuits.

In conclusion, we reported a fabrication route that allows nanopores with different conical shapes to be obtained that consist fully of dielectric oxides. This is a key advancement in terms of nanopore shape and material, since it avoids typical shortcomings of polymer nanopores, which are contamination of the analytes, low stability under harsh conditions and over long-time scales, and low refractive index and dielectric constant that result in lower performance in optics and electronics. In this sense, our approach integrates the advantages of glass-pipette nanopores that are only available on the macroscale to on-chip technologies that enable parallel processing by microarrays of nanopores and their integration in microfluidics. The chemical robustness and high dielectric constant of the metal oxides that are available for ALD also open the way to integrate nanoplasmonics[72] and Mie-tronics with such an on-chip nanopore platform. We demonstrated the excellent properties of the conical dielectric oxide nanopores in ionic current rectification, where they allowed reaching high rectification ratios even for relatively large pore diameters of 50–70 nm, and finite element method simulations elucidated the shape effects on the ionic current flow. We further demonstrated improved performance in electrical detection of DNA translocation of the conical nanopores compared to

https://doi.org/10.1021/acs.nanolett.4c02117
Nano Lett. XXXX, XXX, XXX−XXX

cylindrical ones and connected the asymmetry in ionic current flow and conductance to the hysteresis that we observed in cyclic voltammetry. These insights showed that asymmetric shapes such as concave and convex nanopores are favorable for achieving hysteresis and memristive behavior, which allows designing nanopores for ionic memristor devices that have the best possible properties for the targeted applications, for example, in neuromorphic computing. Therefore, our work opens up new possibilities for exploring the physics and applications of conical nanopores, such as sensing,[73] sequencing,[74,75] nanofluidics,[76] nanoelectronics,[77] and energy harvesting.[78] With the addition of a metallic layer, the versatility of our method allows for the design of tunable plasmonic antennas for enhanced optical techniques.[72,79] Furthermore, exploiting the ability to fabricate 3D nanopores in different materials with high refractive index paves the way to the design and integration of all dielectric nanoresonators, extending the applications of 3D nanopores into Mie-tronics.[80,81]

■ ASSOCIATED CONTENT

Supporting Information

The Supporting Information is available free of charge at https://pubs.acs.org/doi/10.1021/acs.nanolett.4c02117.

Section 1: Nanopore Fabrication and Nanopores from Different Materials; Section 2: Electrical Measurement Details; Section 3: Simulations − Details of the COMSOL modeling; Section 4: Methods and Materials (PDF)

■ AUTHOR INFORMATION

Corresponding Authors

Denis Garoli − *Optoelectronics, Istituto Italiano di Tecnologia, 16163 Genova, Italy; Dipartimento di Scienze e Metodi dell'Ingegneria, Università degli Studi di Modena e Reggio Emilia, 43122 Reggio Emilia, Italy;* orcid.org/0000-0002-5418-7494; Email: denis.garoli@unimore.it

Roman Krahne − *Optoelectronics, Istituto Italiano di Tecnologia, 16163 Genova, Italy;* orcid.org/0000-0003-0066-7019; Email: roman.krahne@iit.it

Authors

German Lanzavecchia − *Optoelectronics, Istituto Italiano di Tecnologia, 16163 Genova, Italy; Dipartimento di Fisica, Università degli Studi di Genova, 16146 Genova, Italy*

Anastasiia Sapunova − *Optoelectronics, Istituto Italiano di Tecnologia, 16163 Genova, Italy; Università degli Studi di Milano-Bicocca, 20126 Milano, Italy*

Ali Douaki − *Optoelectronics, Istituto Italiano di Tecnologia, 16163 Genova, Italy;* orcid.org/0000-0003-1783-5445

Shukun Weng − *Optoelectronics, Istituto Italiano di Tecnologia, 16163 Genova, Italy; Università degli Studi di Milano-Bicocca, 20126 Milano, Italy*

Dmitry Momotenko − *Institute of Chemistry, Carl von Ossietzky Universität Oldenburg, Oldenburg D-26129, Germany*

Gonçalo Paulo − *Dipartimento di Ingegneria Meccanica e Aerospaziale, Sapienza Università di Roma, 00184 Roma, Italy;* orcid.org/0000-0002-2002-884X

Alberto Giacomello − *Dipartimento di Ingegneria Meccanica e Aerospaziale, Sapienza Università di Roma, 00184 Roma, Italy;* orcid.org/0000-0003-2735-6982

Complete contact information is available at: https://pubs.acs.org/10.1021/acs.nanolett.4c02117

Author Contributions

GL conceived the fabrication method, performed the fabrication, and prepared the manuscript, AS and DM performed the numerical simulations, AD, SW, GP, and AG performed the memristor characterization, and RK and DG supervised the work.

Notes

The authors declare no competing financial interest.

■ ACKNOWLEDGMENTS

The authors acknowledge funding from the European Union under the Horizon 2020 Program, FET-Open: DNA-FAIRY-LIGHTS, Grant Agreement 964995, the HORIZON-MSCA-DN-2022: DYNAMO, grant Agreement 101072818. The authors thank the Clean Room Facility of IIT for the support in sample fabrication.

■ REFERENCES

(1) Kasianowicz, J. J.; Brandin, E.; Branton, D.; Deamer, D. W. Characterization of Individual Polynucleotide Molecules Using a Membrane Channel. *Proc. Natl. Acad. Sci. U. S. A.* **1996**, *93* (24), 13770−13773.

(2) Xue, L.; Yamazaki, H.; Ren, R.; Wanunu, M.; Ivanov, A. P.; Edel, J. B. Solid-State Nanopore Sensors. *Nat. Rev. Mater.* **2020**, *5* (12), 931−951.

(3) Hu, R.; Tong, X.; Zhao, Q. Four Aspects about Solid-State Nanopores for Protein Sensing: Fabrication, Sensitivity, Selectivity, and Durability. *Adv. Healthc Mater.* **2020**, *9* (17), 2000933.

(4) Bocquet, L. Nanofluidics Coming of Age. *Nat. Mater.* **2020**, *19* (3), 254−256.

(5) Stein, D.; Kruithof, M.; Dekker, C. Surface-Charge-Governed Ion Transport in Nanofluidic Channels. *Phys. Rev. Lett.* **2004**, *93* (3), 035901.

(6) Acar, E. T.; Buchsbaum, S. F.; Combs, C.; Fornasiero, F.; Siwy, Z. S. Biomimetic Potassium-Selective Nanopores. *Sci. Adv.* **2024**, *5* (2), eaav2568.

(7) Di Muccio, G.; Morozzo Della Rocca, B.; Chinappi, M. Geometrically Induced Selectivity and Unidirectional Electroosmosis in Uncharged Nanopores. *ACS Nano* **2022**, *16* (6), 8716−8728.

(8) Chernev, A.; Teng, Y.; Thakur, M.; Boureau, V.; Navratilova, L.; Cai, N.; Chen, T.-H.; Wen, L.; Artemov, V.; Radenovic, A. Nature-Inspired Stalactite Nanopores for Biosensing and Energy Harvesting. *Adv. Mater.* **2023**, *35* (33), 2302827.

(9) Tsutsui, M.; Hsu, W. L.; Yokota, K.; Leong, I. W.; Daiguji, H.; Kawai, T. Scalability of Nanopore Osmotic Energy Conversion. *Exploration* **2024**, *4* (2), 20220110.

(10) Wang, L.; Wang, Z.; Patel, S. K.; Lin, S.; Elimelech, M. Nanopore-Based Power Generation from Salinity Gradient: Why It Is Not Viable. *ACS Nano* **2021**, *15* (3), 4093−4107.

(11) Teng, Y.; Liu, P.; Fu, L.; Kong, X.-Y.; Jiang, L.; Wen, L. Bioinspired Nervous Signal Transmission System Based on Two-Dimensional Laminar Nanofluidics: From Electronics to Ionics. *Proc. Natl. Acad. Sci. U. S. A.* **2020**, *117* (29), 16743−16748.

(12) Ramirez, P.; Gómez, V.; Cervera, J.; Mafe, S.; Bisquert, J. Synaptical Tunability of Multipore Nanofluidic Memristors. *J. Phys. Chem. Lett.* **2023**, *14* (49), 10930−10934.

(13) Dekker, C. Solid-State Nanopores. *Nat. Nanotechnol* **2007**, *2* (4), 209−215.

(14) Zhao, X.; Qin, H.; Tang, M.; Zhang, X.; Qing, G. Nanopore: Emerging for Detecting Protein Post-Translational Modifications. *TrAC, Trends in Analytical Chemistry* **2024**, *173*, 117658.

(15) Bleidorn, C. Third Generation Sequencing: Technology and Its Potential Impact on Evolutionary Biodiversity Research. *Syst. Biodivers* **2016**, *14* (1), 1−8.

(16) Doricchi, A.; Platnich, C. M.; Gimpel, A.; Horn, F.; Earle, M.; Lanzavecchia, G.; Cortajarena, A. L.; Liz-Marzan, L. M.; Liu, N.; Heckel, R.; Grass, R. N.; Krahne, R.; Keyser, U. F.; Garoli, D. Emerging Approaches to DNA Data Storage: Challenges and Prospects. *ACS Nano* **2022**, *16* (11), 17552−17571.
(17) Thakur, M.; Cai, N.; Zhang, M.; Teng, Y.; Chernev, A.; Tripathi, M.; Zhao, Y.; Macha, M.; Elharouni, F.; Lihter, M.; Wen, L.; Kis, A.; Radenovic, A. High Durability and Stability of 2D Nanofluidic Devices for Long-Term Single-Molecule Sensing. *NPJ. 2D Mater. Appl.* **2023**, *7* (1), 11.
(18) He, Y.; Tsutsui, M.; Zhou, Y.; Miao, X.-S. Solid-State Nanopore Systems: From Materials to Applications. *NPG Asia Mater.* **2021**, *13* (1), 48.
(19) Liang, S.; Xiang, F.; Tang, Z.; Nouri, R.; He, X.; Dong, M.; Guan, W. Noise in Nanopore Sensors: Sources, Models, Reduction, and Benchmarking. *Nanotechnology and Precision Engineering* **2020**, *3* (1), 9−17.
(20) Yi, W.; Zhang, C.; Zhang, Q.; Zhang, C.; Lu, Y.; Yi, L.; Wang, X. Solid-State Nanopore/Nanochannel Sensing of Single Entities. *Top Curr. Chem.* **2023**, *381* (4), 13.
(21) Chen, Q.; Liu, Z. Fabrication and Applications of Solid-State Nanopores. *Sensors (Switzerland)* 2019, DOI: 10.3390/s19081886.
(22) Healy, K.; Schiedt, B.; Morrison, A. P. Solid-State Nanopore Technologies for Nanopore-Based DNA Analysis. *Nanomedicine* **2007**, *2* (6), 875−897.
(23) Chuang, P. Y.; Hsu, J. P. Influence of Shape and Charged Conditions of Nanopores on Their Ionic Current Rectification, Electroosmotic Flow, and Selectivity. *Colloids Surf. A Physicochem Eng. Asp* **2023**, *658*, 130696.
(24) Tseng, S.; Lin, S.-C.; Lin, C.-Y.; Hsu, J.-P. Influences of Cone Angle and Surface Charge Density on the Ion Current Rectification Behavior of a Conical Nanopore. *J. Phys. Chem. C* **2016**, *120* (44), 25620−25627.
(25) Cruz-Chu, E. R.; Aksimentiev, A.; Schulten, K. Ionic Cürrent Rectification through Silica Nanopores. *J. Phys. Chem. C* **2009**, *113* (5), 1850−1862.
(26) Wen, C.; Zeng, S.; Li, S.; Zhang, Z.; Zhang, S. L. On Rectification of Ionic Current in Nanopores. *Anal. Chem.* **2019**, *91* (22), 14597−14604.
(27) Trivedi, M.; Nirmalkar, N. Ion Transport and Current Rectification in a Charged Conical Nanopore Filled with Viscoelastic Fluids. *Sci. Rep* **2022**, *12* (1), DOI: 10.1038/s41598-022-06079-w.
(28) Ai, Y.; Zhang, M.; Joo, S. W.; Cheney, M. A.; Qian, S. Effects of Electroosmotic Flow on Ionic Current Rectification in Conical Nanopores. *J. Phys. Chem. C* **2010**, *114* (9), 3883−3890.
(29) Wang, D.; Kvetny, M.; Liu, J.; Brown, W.; Li, Y.; Wang, G. Transmembrane Potential across Single Conical Nanopores and Resulting Memristive and Memcapacitive Ion Transport. *J. Am. Chem. Soc.* **2012**, *134* (8), 3651−3654.
(30) He, Y.; Tsutsui, M.; Zhou, Y.; Miao, X.-S. Solid-State Nanopore Systems: From Materials to Applications. *NPG Asia Mater.* **2021**, *13* (1), 48.
(31) Paulo, G.; Sun, K.; Di Muccio, G.; Gubbiotti, A.; Morozzo della Rocca, B.; Geng, J.; Maglia, G.; Chinappi, M.; Giacomello, A. Hydrophobically Gated Memristive Nanopores for Neuromorphic Applications. *Nat. Commun.* **2023**, *14* (1), 8390.
(32) Lee, J.; Du, C.; Sun, K.; Kioupakis, E.; Lu, W. D. Tuning Ionic Transport in Memristive Devices by Graphene with Engineered Nanopores. *ACS Nano* **2016**, *10* (3), 3571−3579.
(33) Spende, A.; Sobel, N.; Lukas, M.; Zierold, R.; Riedl, J. C.; Gura, L.; Schubert, I.; Moreno, J. M. M.; Nielsch, K.; Stühn, B.; Hess, C.; Trautmann, C.; Toimil-Molares, M. E. TiO2, SiO2, and Al2O3 Coated Nanopores and Nanotubes Produced by ALD in Etched Ion-Track Membranes for Transport Measurements. *Nanotechnology* **2015**, *26* (33), 335301.
(34) Fragasso, A.; Schmid, S.; Dekker, C. Comparing Current Noise in Biological and Solid-State Nanopores. *ACS Nano* **2020**, *14* (2), 1338−1349.
(35) Chen, K.; Choudhary, A.; Sandler, S. E.; Maffeo, C.; Ducati, C.; Aksimentiev, A.; Keyser, U. F. Super-Resolution Detection of DNA Nanostructures Using a Nanopore. *Adv. Mater.* **2023**, *35* (12), 2207434.
(36) Roman, J.; Français, O.; Jarroux, N.; Patriarche, G.; Pelta, J.; Bacri, L.; Le Pioufle, B. Solid-State Nanopore Easy Chip Integration in a Cheap and Reusable Microfluidic Device for Ion Transport and Polymer Conformation Sensing. *ACS Sens* **2018**, *3* (10), 2129−2137.
(37) Gadaleta, A.; Sempere, C.; Gravelle, S.; Siria, A.; Fulcrand, R.; Ybert, C.; Bocquet, L. Sub-Additive Ionic Transport across Arrays of Solid-State Nanopores. *Phys. Fluids* **2014**, *26* (1), 012005.
(38) De Angelis, F.; Malerba, M.; Patrini, M.; Miele, E.; Das, G.; Toma, A.; Zaccaria, R. P.; Di Fabrizio, E. 3D Hollow Nanostructures as Building Blocks for Multifunctional Plasmonics. *Nano Lett.* **2013**, *13* (8), 3553−3558.
(39) Zhu, L.; Yang, G. L.; Ding, W. J.; Cao, Y. Q.; Li, W. M.; Li, A. D. Growth Behavior of Ir Metal Formed by Atomic Layer Deposition in the Nanopores of Anodic Aluminum Oxide. *Dalton Transactions* **2022**, *51* (25), 9664−9672.
(40) Chen, P.; Mitsui, T.; Farmer, D. B.; Golovchenko, J.; Gordon, R. G.; Branton, D. Atomic Layer Deposition to Fine-Tune the Surface Properties and Diameters of Fabricated Nanopores. *Nano Lett.* **2004**, *4* (7), 1333−1337.
(41) Garoli, D.; Zilio, P.; De Angelis, F.; Gorodetski, Y. Helicity Locking of Chiral Light Emitted from a Plasmonic Nanotaper. *Nanoscale* **2017**, *9* (21), 6965−6969.
(42) Garoli, D.; Zilio, P.; Gorodetski, Y.; Tantussi, F.; De Angelis, F. Beaming of Helical Light from Plasmonic Vortices via Adiabatically Tapered Nanotip. *Nano Lett.* **2016**, *16* (10), 6636−6643.
(43) Knoops, H. C. M.; Braeken, E. M. J.; De Peuter, K.; Potts, S. E.; Haukka, S.; Pore, V.; Kessels, W. M. M. Atomic Layer Deposition of Silicon Nitride from Bis(Tert-Butylamino)Silane and N2 Plasma. *ACS Appl. Mater. Interfaces* **2015**, *7* (35), 19857−19862.
(44) Zhang, X. Y.; Yang, Y.; Zhang, Z. X.; Geng, X. P.; Hsu, C. H.; Wu, W. Y.; Lien, S. Y.; Zhu, W. Z. Deposition and Characterization of Rp ald Sio2 Thin Films with Different Oxygen Plasma Powers. *Nanomaterials* **2021**, *11* (5), 1173.
(45) Zelentsov, S. V.; Zelentsova, N. V.; Kolesov, A. N.; Bogatyreva, L. A.; Mashtakov, I. A. Enhancing the Dry-Etch Durability of Photoresist Masks: A Review of the Main Approaches. *Russian Microelectronics* **2007**, *36* (1), 40−48.
(46) West, A.; Van Der Schans, M.; Xu, C.; Cooke, M.; Wagenaars, E. Fast, Downstream Removal of Photoresist Using Reactive Oxygen Species from the Effluent of an Atmospheric Pressure Plasma Jet. *Plasma Sources Sci. Technol.* **2016**, *25* (2), 02LT01.
(47) Le, Q. T.; Kesters, E.; Prager, L.; Claes, M.; Lux, M.; Vereecke, G. Modification of Photoresist by UV for Post-Etch Wet Strip Applications. *Solid State Phenomena* **2009**, *145−146*, 323−326.
(48) Bauer, J.; Crook, C.; Baldacchini, T. A Sinterless, Low-Temperature Route to 3D Print Nanoscale Optical-Grade Glass. *Science (1979)* **2023**, *380* (6648), 960−966.
(49) Dingemans, G.; van Helvoirt, C. A. A.; Pierreux, D.; Keuning, W.; Kessels, W. M. M. Plasma-Assisted ALD for the Conformal Deposition of SiO 2 : Process, Material and Electronic Properties. *J. Electrochem. Soc.* **2012**, *159* (3), H277−H285.
(50) Aristanti, Y.; Supriyatna, Y. I.; Masduki, N. P.; Soepriyanto, S. Effect of Calcination Temperature on the Characteristics of TiO_2 Synthesized from Ilmenite and Its Applications for Photocatalysis. *IOP Conf Ser. Mater. Sci. Eng.* **2019**, *478*, 012019.
(51) Barsukova, M. G.; Shorokhov, A. S.; Musorin, A. I.; Neshev, D. N.; Kivshar, Y. S.; Fedyanin, A. A. Magneto-Optical Response Enhanced by Mie Resonances in Nanoantennas. *ACS Photonics* **2017**, *4* (10), 2390−2395.
(52) Kruk, S.; Kivshar, Y. Functional Meta-Optics and Nanophotonics Governed by Mie Resonances. *ACS Photonics* **2017**, *4* (11), 2638−2649.
(53) Cervera, J.; Schiedt, B.; Neumann, R.; Mafá, S.; Ramírez, P. Ionic Conduction, Rectification, and Selectivity in Single Conical Nanopores. *J. Chem. Phys.* **2006**, *124* (10), 104706.

https://doi.org/10.1021/acs.nanolett.4c02117
Nano Lett. XXXX, XXX, XXX−XXX

(54) Kiy, A.; Dutt, S.; Notthoff, C.; Toimil-Molares, M. E.; Kirby, N.; Kluth, P. Highly Rectifying Conical Nanopores in Amorphous SiO2Membranes for Nanofluidic Osmotic Power Generation and Electroosmotic Pumps. *ACS Appl. Nano Mater.* **2023**, *6* (10), 8564−8573.
(55) Gubbiotti, A.; Baldelli, M.; Di Muccio, G.; Malgaretti, P.; Marbach, S.; Chinappi, M. Electroosmosis in Nanopores: Computational Methods and Technological Applications. *Adv. Phys. X* **2022**, *7* (1), 2036638.
(56) Bruus, H. *Theoretical Microfluidics*, 2007th ed.; Oxford Academic, 1997; Vol. *18*, DOI: 10.1093/oso/9780199235087.001.0001.
(57) Kubeil, C.; Bund, A. The Role of Nanopore Geometry for the Rectification of Ionic Currents. *J. Phys. Chem. C* **2011**, *115* (16), 7866−7873.
(58) Apel, P. Y.; Blonskaya, I. V.; Orelovitch, O. L.; Ramirez, P.; Sartowska, B. A. Effect of Nanopore Geometry on Ion Current Rectification. *Nanotechnology* **2011**, *22* (17), 175302.
(59) Thangaraj, V.; Lepoitevin, M.; Smietana, M.; Balanzat, E.; Bechelany, M.; Janot, J. M.; Vasseur, J. J.; Subramanian, S.; Balme, S. Detection of Short SsDNA and DsDNA by Current-Voltage Measurements Using Conical Nanopores Coated with Al2O3 by Atomic Layer Deposition. *Microchimica Acta* **2016**, *183* (3), 1011−1017.
(60) Tseng, S.; Lin, S. C.; Lin, C. Y.; Hsu, J. P. Influences of Cone Angle and Surface Charge Density on the Ion Current Rectification Behavior of a Conical Nanopore. *J. Phys. Chem. C* **2016**, *120* (44), 25620−25627.
(61) Niedzwiecki, D. J.; Chou, Y. C.; Xia, Z.; Thei, F.; Drndić, M. Detection of Single Analyte and Environmental Samples with Silicon Nitride Nanopores: Antarctic Dirt Particulates and DNA in Artificial Seawater. *Rev. Sci. Instrum.* **2020**, *91* (3), 031301.
(62) Lanzavecchia, G.; Kuttruff, J.; Doricchi, A.; Douaki, A.; Kumaranchira Ramankutty, K.; García, I.; Lin, L.; Viejo Rodríguez, A.; Wågberg, T.; Krahne, R.; Maccaferri, N.; Garoli, D. Plasmonic Photochemistry as a Tool to Prepare Metallic Nanopores with Controlled Diameter for Optimized Detection of Single Entities. *Adv. Opt Mater.* **2023**, *11* (16), 2300786.
(63) Noh, Y.; Smolyanitsky, A. Memristive Response and Capacitive Spiking in Aqueous Ion Transport through Two-Dimensional Nanopore Arrays. *J. Phys. Chem. Lett.* **2024**, *15* (3), 665−670.
(64) Hou, Y.; Hou, X. Bioinspired Nanofluidic Iontronics. *Science (1979)* **2021**, *373* (6555), 628−629.
(65) Liu, W.; Mei, T.; Cao, Z.; Li, C.; Wu, Y.; Wang, L.; Xu, G.; Chen, Y.; Zhou, Y.; Wang, S.; Xue, Y.; Yu, Y.; Kong, X.-Y.; Chen, R.; Tu, B.; Xiao, K. Bioinspired Carbon Nanotube-Based Nanofluidic Ionic Transistor with Ultrahigh Switching Capabilities for Logic Circuits. *Sci. Adv.* **2024**, *10* (11), eadj7867.
(66) Roy, K.; Jaiswal, A.; Panda, P. Towards Spike-Based Machine Intelligence with Neuromorphic Computing. *Nature* **2019**, *575* (7784), 607−617.
(67) Marković, D.; Mizrahi, A.; Querlioz, D.; Grollier, J. Physics for Neuromorphic Computing. *Nature Reviews Physics* **2020**, *2* (9), 499−510.
(68) Chua, L. If It's Pinched It's a Memristor. *Semicond. Sci. Technol.* **2014**, *29* (10), 104001.
(69) Ramirez, P.; Portillo, S.; Cervera, J.; Bisquert, J.; Mafe, S. Memristive Arrangements of Nanofluidic Pores. *Phys. Rev. E* **2024**, *109* (4), 44803.
(70) Kamsma, T. M.; Kim, J.; Kim, K.; Boon, W. Q.; Spitoni, C.; Park, J.; van Roij, R. Brain-Inspired Computing with Fluidic Iontronic Nanochannels. *Proc. Natl. Acad. Sci. U. S. A.* **2024**, *121* (18), e2320242121.
(71) Kamsma, T. M.; Boon, W. Q.; ter Rele, T.; Spitoni, C.; van Roij, R. Iontronic Neuromorphic Signaling with Conical Microfluidic Memristors. *Phys. Rev. Lett.* **2023**, *130* (26), 268401.
(72) Li, W.; Zhou, J.; Maccaferri, N.; Krahne, R.; Wang, K.; Garoli, D. Enhanced Optical Spectroscopy for Multiplexed DNA and Protein-Sequencing with Plasmonic Nanopores: Challenges and Prospects. *Anal. Chem.* **2022**, *94* (2), 503−514.
(73) Storm, A. J.; Chen, J. H.; Ling, X. S.; Zandbergen, H. W.; Dekker, C. Fabrication of Solid-State Nanopores with Single-Nanometre Precision. *Nat. Mater.* **2003**, *2* (8), 537−540.
(74) Lee, K.; Park, K.-B.; Kim, H.-J.; Yu, J.-S.; Chae, H.; Kim, H.-M.; Kim, K.-B. Recent Progress in Solid-State Nanopores. *Adv. Mater.* **2018**, *30* (42), 1704680.
(75) Dorey, A.; Howorka, S. Nanopore DNA Sequencing Technologies and Their Applications towards Single-Molecule Proteomics. *Nat. Chem.* **2024**, *16* (3), 314−334.
(76) Pérez-Mitta, G.; Toimil-Molares, M. E.; Trautmann, C.; Marmisollé, W. A.; Azzaroni, O. Molecular Design of Solid-State Nanopores: Fundamental Concepts and Applications. *Adv. Mater.* **2019**, *31* (37), 1901483.
(77) Krapf, D.; Wu, M.-Y.; Smeets, R. M. M.; Zandbergen, H. W.; Dekker, C.; Lemay, S. G. Fabrication and Characterization of Nanopore-Based Electrodes with Radii down to 2 Nm. *Nano Lett.* **2006**, *6* (1), 105−109.
(78) Feng, J.; Graf, M.; Liu, K.; Ovchinnikov, D.; Dumcenco, D.; Heiranian, M.; Nandigana, V.; Aluru, N. R.; Kis, A.; Radenovic, A. Single-Layer MoS2 Nanopores as Nanopower Generators. *Nature* **2016**, *536* (7615), 197−200.
(79) Garoli, D.; Yamazaki, H.; Maccaferri, N.; Wanunu, M. Plasmonic Nanopores for Single-Molecule Detection and Manipulation: Toward Sequencing Applications. *Nano Lett.* **2019**, *19* (11), 7553−7562.
(80) Koshelev, K.; Kruk, S.; Melik-Gaykazyan, E.; Choi, J.-H.; Bogdanov, A.; Park, H.-G.; Kivshar, Y. Subwavelength Dielectric Resonators for Nonlinear Nanophotonics. *Science (1979)* **2020**, *367* (6475), 288−292.
(81) Kivshar, Y. The Rise of Mie-Tronics. *Nano Lett.* **2022**, *22* (9), 3513−3515.

https://doi.org/10.1021/acs.nanolett.4c02117
Nano Lett. XXXX, XXX, XXX−XXX